PCCP

ROYAL SOCIETY OF CHEMISTRY

PAPER

Cite this: *Phys. Chem. Chem. Phys.*, 2026, **28**, 5516

Astrochemistry prefers the biomolecule: isomer-selective production of ethanolamine ($HOCH_2CH_2NH_2$) in interstellar model ices

Joshua H. Marks,†[ab] Anatoliy A. Nikolayev,†[c] Jia Wang,†[ab] Ivan O. Antonov,[c] Alexander M. Mebel*[d] and Ralf I. Kaiser*[ab]

Received 29th November 2025,
Accepted 16th January 2026

DOI: 10.1039/d5cp04639d

rsc.li/pccp

A crucial molecule in the chemistry of life, ethanolamine ($HOCH_2CH_2NH_2$) is among the most prevalent biomolecules. It serves as a ubiquitous hydrophilic head group for the molecules comprising cellular membranes and it functions as both precursor and intermediate in the biological synthesis of neurotransmitters among other metabolites, protein folding, and post-translational modification. Because of the out-sized biological importance of this molecule ethanolamine is expected to serve as a signature for prebiotic chemistry in space, highlighting the importance of its recent discovery. Here, we show that model interstellar ices containing methanol (CH_3OH) and methylamine (CH_3NH_2) produce ethanolamine upon exposure to an environment simulating that of dense interstellar molecular clouds. Ethanolamine was identified in the gas phase during temperature-programmed desorption utilizing vacuum ultraviolet photoionization reflectron time-of-flight mass spectrometry. Despite irradiation by electrons with energy far exceeding any covalent interaction, reactions toward C_2H_7NO isomers are selective for ethanolamine while its isomers are not detected. Computations provide support that polar solvation destabilizes nitrogen- and oxygen-centered radicals while lowering the barrier to intramolecular hydrogen transfer, resulting in the selective stabilization and formation of carbon-centered radicals. These findings explain the unexpected abundance of ethanolamine in the interstellar medium, and the apparent isomer-selectivity of this reaction may represent a mechanism by which ice-phase astrochemical reactions are preferential toward the building blocks of life.

Introduction

The prevalence of phospholipid cellular membranes—$CH_2R'CHRCH_2OPO_3R''$ where R and R′ are fatty acids (*e.g.*, $CH_3(CH_2)_{2n}COOH$) and R″ a hydrophilic head-group (Scheme 1)—across all contemporary lifeforms signifies their early adoption during the origins of life.[3,4] A key necessity of the field of astrochemistry is to reveal intersections between the chemical composition of the interstellar medium (ISM) and biochemistry through studying the chemical reactions of the ISM and how they contribute to the chemical building-blocks of life, *i.e.*, proteinogenic amino acids ($NH_2CHRCOOH$), phosphate (PO_4^{3-}), sugars ($C_n(H_2O)_n$), nucleobases (purines/pyrimidines), fatty acids (RCOOH), glycerol ($HOCH_2CH(OH)CH_2OH$), and hydrophilic head groups, *e.g.*, ethanolamine ($H_2NCH_2CH_2OH$, **1**), choline ($HOCH_2CH_2N^+(CH_3)_3$), or serine ($H_2NCH(CH_2OH)COOH$).[3,5] Phosphatidylethanolamines comprise the simplest class of phospholipids composed of fatty acids and ethanolamine bound to glycerol (Scheme 1),[6] and serve vital roles beyond the cell membrane such as in neurotransmitter synthesis,[7,8] transmembrane protein folding,[9–11] and function as metabolic reservoirs of ethanolamine (**1**) for post-translational modification of proteins and the biosynthesis of numerous metabolites.[12–15] The pathways by which ethanolamine (**1**) is produced biologically (Scheme 1)[2,16–18] are too complex to have been achievable by nascent life on early Earth. The lack of complex biochemistry in primitive lifeforms demands alternative explanations for the source of these molecular building blocks of life. The formation of biomolecules like ethanolamine (**1**) in the interstellar medium (ISM) constitutes a critical condition for the development of life.[3] Molecular clouds are composed of ice-coated nanoparticles with number densities of only 10^{-11} cm^{-3}.[19] These clouds are typically 10^2–10^7 times more massive than the sun, and the number and density of particles effectively shields their interior from the

[a] *Department of Chemistry, University of Hawaii at Manoa, Honolulu, HI 96822, USA. E-mail: ralfk@hawaii.edu*
[b] *W. M. Keck Research Laboratory in Astrochemistry, University of Hawaii at Manoa, Honolulu, HI 96822, USA*
[c] *Samara University, Samara 443086, Russia*
[d] *Department of Chemistry and Biochemistry, Florida International University, Miami, Florida 33199, USA. E-mail: mebela@fiu.edu*
† These authors contributed equally to this work.

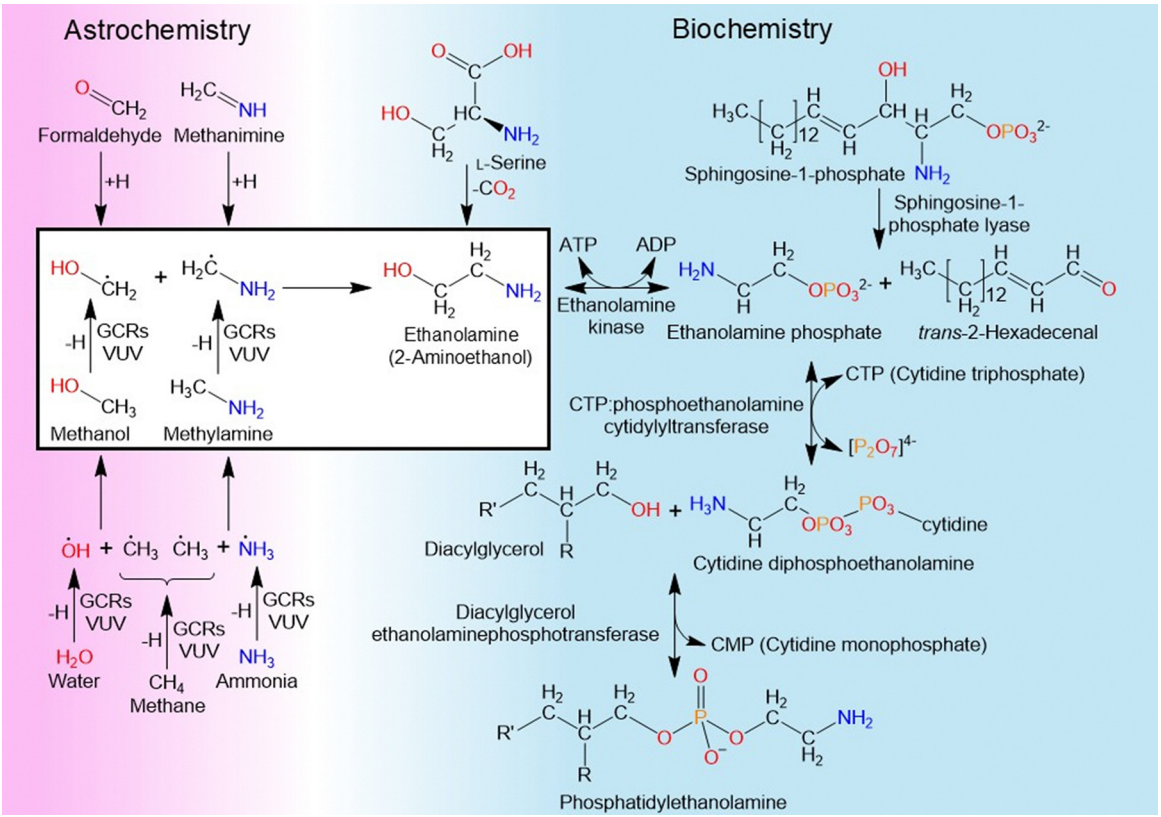

Scheme 1 A comparison between example astrochemical[1] and biochemical[2] synthesis of ethanolamine. Small simple molecules dominate the chemistry of the interstellar medium, making bottom-up reaction mechanisms a far more likely explanation for the presence of complex organics. In contrast, ethanolamine is accessed biochemically only *via* top-down chemistry like the reactions provided as an example above.

light and heat of nearby stars resulting in an extremely cold environment.[19] The icy particles are exposed to galactic cosmic rays (GCRs) which pass through the clouds producing large numbers of energetic secondary electrons and triggering the chemistry of these "molecular factories."[20] This environment supports the non-equilibrium formation and growth of increasingly complex organics including biologically active molecules such as sugars and amino acids.[21,22] The delivery of ethanolamine (**1**) produced in deep space to the oceans of the early Earth during Archean Eon (4 Billion years ago) by comets and/or meteorites presents a viable explanation for origin of the chemical prerequisites for life to develop.[3]

The importance of ethanolamine (**1**) to astrobiology cannot be overstated. It is one of the simplest molecules to share the NCCO backbone with proteinogenic amino acids and may represent an efficient route to their abiotic production in the ISM.[23] This molecule has been the subject of spectroscopic,[24–27] astronomical,[28–30] and laboratory investigations of model interstellar ices.[31] Experiments which simulate the temperature, pressure, and observed chemical composition of dense molecular clouds produce a large variety of biorelevant products such as amino acids,[21] sugars,[32,33] sugar acids,[34] glycerol,[35,36] phosphates,[37] and even glycerol phosphates,[38] but the combination of *ex situ* identification and the complexity of the mixture of organics produced in these simulations leaves unclear if products like ethanolamine (**1**) form under astrophysical conditions. Exposure to atmosphere and destructive chemical analysis prevents extraction of mechanistic information, and a better understanding of the chemical mechanisms represented is key to our understanding of the exotic chemistry of the ISM. The recent discovery of ethanolamine (**1**) in deep space by Rivilla *et al.* marks a major advancement for astrobiology,[30] and its surprising abundance in the G+0.693–0.027 molecular cloud, a part of the Sagittarius B2 molecular cloud complex in the Milky Way's center, indicates the efficiency of the reactions leading to its production. Its large dipole moment of 3.05 ± 0.05 D[39] and prime importance in terrestrial biochemistry labels ethanolamine (**1**) as a readily detectable tracer for astrochemistry with the potential to lead to life. The formation pathways responsible for its presence are unknown, but its production and later incorporation into circumstellar bodies is evidenced by its detection in the Almahata Sitta meteorite.[40]

Methanol (CH_3OH) and methylamine (CH_3NH_2) have both been detected in the ISM and are ideal reactants to facilitate these laboratory astrochemical investigation of the formation of 2-aminoethanol.[45–47] The simplified chemical composition of model ices employed in these experiments permits clear identification of ethanolamine (**1**) and its formation mechanism under energetic irradiation (Fig. 1). Experimental conditions simulate the pressure and temperature of the molecular cloud environment while an electron gun simulates the effects

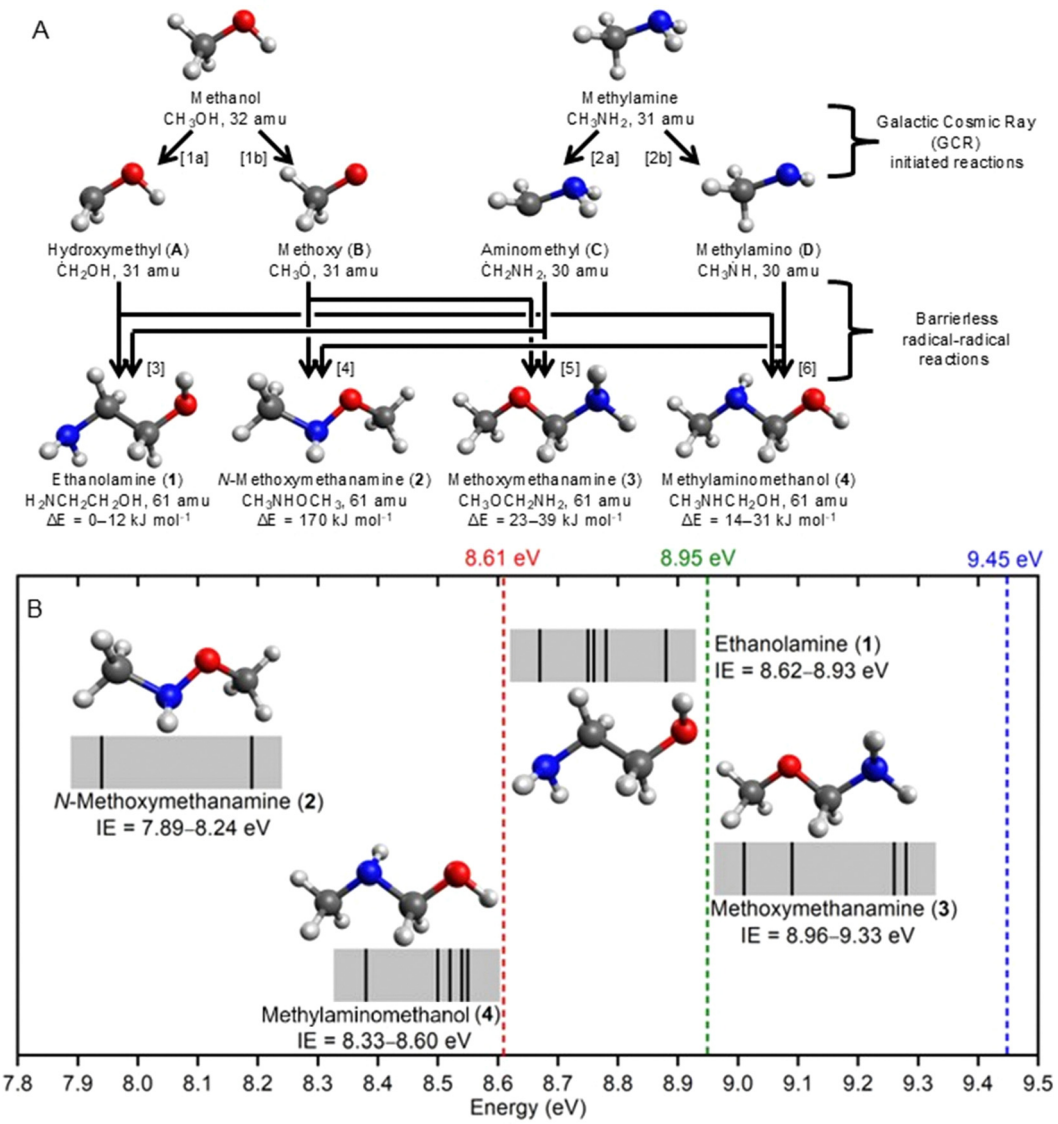

Fig. 1 (A) Isomers of C_2H_7NO achievable through Ḣ elimination initiated by an incident electron simulating secondary electrons produced in the track of a galactic cosmic ray (GCR) followed by radical–radical recombination. Products are labelled with structural molecular formulae, molecular mass (atomic mass units, amu), and relative energy (ΔE) with reference to the minimum energy isomer identified. (B) Calculated adiabatic ionization energies (IEs) for each isomer of C_2H_7NO are indicated by the black lines, one for each conformer, and include a −0.03 eV Stark effect correction.[41,42] The gray areas display ±0.05 eV error and represent the range over which adiabatic ionization is possible for all conformers of each structural isomer.[43,44] Vertical dashed lines indicate three selected VUV photon energies chosen to distinguish among isomers ethanolamine (**1**), methoxymethanamine (**3**), and methylaminoethanol (**4**).

of GCRs impacting the cloud. Radical reactions are found to predominate and recombination of larger radicals leads to the formation of increasingly complex organics.[48] Temperature-programmed desorption (TPD) following irradiation simulates the transition of a cold molecular cloud to a warm star-forming region and results in the gradual sublimation of radiolysis products.[19] These products are then detected in the gas phase by photoionization reflectron time-of-flight mass spectrometry (PI-ReToF-MS). The predicted ionization energy of ethanolamine (**1**) (Fig. 1) is unique among the accessible isomers (Fig. S1 and Tables S1–S4): *N*-methoxymethanamine (CH_3NHOCH_3, **2**), methoxymethanamine ($CH_3OCH_2NH_2$, **3**), and methylaminoethanol (CH_3NHCH_2OH, **4**). This permits a facile identification of ethanolamine (**1**) in the gas phase by photoionization reflectron time-of-flight mass spectrometry (PI-ReToF-MS) while isotopic substitution of the reactants permits unambiguous confirmation of the detected molecular formula. To provide a roadmap toward a chemical explanation for the abundance of ethanolamine (**1**) in space, the space simulation experiments detailed here take full advantage of *in situ* and *isomer-specific* detection after model interstellar ices are subjected to conditions simulating the typical temperature, pressure, and radiation field of dense interstellar molecular clouds like Sgr B2.[30] Here, we provide persuasive testimony on a previously elusive bottom-up pathway to

ethanolamine (**1**) involving reactions of relatively stable carbon-centered radicals, *i.e.* hydroxymethyl ($\dot{C}H_2OH$) and aminomethyl ($\dot{C}H_2NH_2$), in interstellar model ices of methanol and methylamine upon exposure to ionizing radiation, thus affording an abiotic mechanism of synthesizing a crucial biomolecule in deep space prior to eventual terrestrial delivery by comets and meteorites.

Experimental methods

The experiments were conducted in a hydrocarbon-free ultra-high vacuum (UHV) chamber evacuated to an ultimate pressure as low as 10^{-11} Torr.[41] The binary ice mixtures (Table S5) were prepared on a mirror polished silver wafer maintained at 5.0 ± 0.2 K by a cold head (Sumitomo Heavy Industries, RDK-415E). The cold head is mounted on a doubly differentially pumped rotating flange and bellows to allow both rotation and translation about or along a central axis. Methanol (CH_3OH, Fisher Scientific, >99.8%; CD_3OH, Sigma-Aldrich, 99.8 atom % D; CD_3OD, Sigma-Aldrich, ≥99.8 atom % D) samples were degassed by a minimum of three freeze–pump–thaw cycles. Leak valves were used to introduce methanol vapor or methylamine gas (CH_3NH_2, 99.5% Matheson TriGas; CD_3ND_2, Cambridge Isotope Laboratories, 98 atom % D) through separate 10 mm diameter glass capillary arrays at a partial pressure of 1.0 ± 0.2 × 10^{-8} Torr each. The progress of the deposition was monitored by observing the effects of thin film interference on the reflected power of a helium-neon laser reflected by the silver wafer.[49] After deposition, Fourier transform infrared (FTIR) spectra were used to determine the relative concentration of methanol and methylamine within the ice. The refractive index of the ice is determined by a weighted average of the 15 K refractive indices of methanol (1.30) methylamine (1.38); this yields ice thicknesses of 735 ± 50 nm.[50]

Ices that were irradiated were exposed to an electron gun producing 5 keV electrons rastered across a 1.6 mm^2 area. This simulates the effects of secondary electrons produced by galactic cosmic rays on interstellar ices.[51] Monte Carlo simulations (CASINO 2.42) of energy transfer by energetic electrons were used to calculate the irradiation dose per molecule and the penetration depth.[52] Rate and duration of electron irradiation was varied throughout the experiment and are detailed in Table S6. Simulations indicate that the average penetration depth of electrons is 340 ± 10 nm into the surface of the ice, much less than the 730 ± 30 nm thickness of the ices employed for these experiments. At this depth approximately 95% of the energy imparted by the electrons has already been absorbed. Ices are deliberately made thicker than the average penetration depth in order to minimize any chemical interactions with the silver substrate.

Following irradiation ices were heated at a rate of 1 K min^{-1} from 5 K to 320 K (temperature-programmed desorption; TPD). Subliming molecules were detected through photoionization reflectron time-of-flight mass spectrometry (PI-ReToF-MS). Four-wave mixing difference frequency generation employing the 222.566 nm two-photon absorption ($2\omega_1$) of Xe was used to produce VUV light with ω_{VUV} energy equal to $2\omega_1$–ω_2. A pair of pulsed dye lasers (Sirah Lasertechnik, Cobra-Stretch) pumped by the second or third harmonics of 30 Hz Nd^{3+}:YAG lasers were used to produce ω_1 and ω_2 where ω_2 was varied to achieve specific VUV photon energies: 733.071 nm for 9.45 eV, 565.803 nm for 8.95 eV, 550.723 nm for 8.89 eV, 489.805 nm for 8.61 eV, and 460.686 nm for 8.45 eV. Fundamentals and unwanted harmonics were separated after VUV production by passing the diverging beams of ω_1, ω_2, and ω_{VUV} through an off-center biconvex lithium fluoride lens and directing only the recollimated VUV light through an aperture. The VUV light passes about 2 mm above the surface of the ice during TPD. This method of VUV production was measured to produce 4 ± 2 × 10^{11} photons s^{-1}. Photoionized molecules were extracted into the ReToF-MS and detected with a multichannel plate after separation based on their mass-to-charge ratios. Ion counting was accomplished by amplifying the signal 100 : 1 before further amplification with a 100 MHz discriminator. Ion time-of-flight was recorded with a multichannel scaler which accumulated signals into 3.2 ns bins for each 2-minute intervals during TPD.

Computational methods

Calculation of adiabatic ionization energies with chemical accuracy is necessary for experimental analysis, as such these calculations are performed at the CBS-QB3 level of theory.[43,44] Geometries of neutral molecules were optimized for all possible combinations of dihedral angles of asymmetric internal rotors, *i.e.* –OH, $–NH_2$, $–CH_2–$, –O–, and –NH–. For ions, starting geometries were taken from the optimized neutral molecules. Molecular parameters of both neutral and cationic states of each conformer were optimized using the CBS-QB3 composite method. This begins with structural optimization and zero-point vibrational energy using the B3LYP hybrid density functional and the 6-311G(2d,d,p) (CBSB7) basis set, providing accuracy of 1–2 pm for bond lengths as well as 1–2° for bond angles. The electronic energy is then extrapolated using CCSD(T) and MP4SDQ *ab initio* calculations resulting in mean absolute error of 5 kJ mol^{-1} and root-mean-square error of 6 kJ mol^{-1} for computed enthalpies of formation for the G2/97 test set, and a mean error of 0.05 eV for computed adiabatic ionization energies.[43,44] The adiabatic ionization energy of each conformer are indicated in Fig. 1 where they include a –0.03 eV correction that is necessary because a combination of the acceleration field of the mass spectrometer (Stark effect) and thermal energy lower the experimentally observable ionization energy predictably.[42] The Gaussian 09 package was utilized for all calculations.[41,53] Additionally, the accuracy of the ionization energies was verified at the explicitly correlated CCSD(T)-F12 level of theory[54,55] extrapolated to the complete basis set (CBS) limit from single-point calculations with the cc-pVTZ-f12 and cc-pVQZ-f12 basis sets and the geometries of the neutral isomers and their ions optimized at the doubly-hybrid density

functional B2PLYPD3[56–58]/aug-cc-pVTZ level. The CCSD(T)-F12 calculations were carried out using the MOLPRO package.[59] The differences between the higher-level CCSD(T)-F12/CBS-(vtz-vqz)//B2PLYPD3/aug-cc-pVTZ values and CBS-QB3 results did not exceed 0.02–0.03 eV (1.9–2.9 kJ mol^{-1}).

A less expensive computational protocol was used for exploration of the potential energy surfaces for reactions of intramolecular hydrogen transfer and intermolecular hydrogen abstraction involving methanol-derived and methylamine-derived radicals with the goal to qualitatively understand the reaction mechanisms and to interpret experimental observations. These calculations were carried out entirely at the ωB97X-D/6-311G(d,p) level of theory and are detailed in Tables S7 and S8. In exploring the effects of explicit solvation, possible combinations of up to three total solvent molecules of methanol and/or methylamine were included. The effects of implicit solvent was treated using the polarizable continuum model (PCM),[60] with solvents representing the electrostatic parameters of liquid methanol,[61] solid methanol,[62] and liquid methylamine.[63] It should be noted that, while this theoretical approach does not fully represent all structural, dynamical, or energetic constraints of amorphous cryogenic ices, such as restricted molecular motion, radical trapping, cage effects, and heterogeneous hydrogen bonding environments, it provides qualitative trends sufficient to put forward a reasonable hypothesis on the reaction mechanism accounting for the experimental observations in this work. All plausible conformers were considered for bimolecular reactions, but only those including direct interactions between hydroxyl and amino groups were found to be stable. All transition states were confirmed by the presence of a single imaginary frequency which corresponded to the reaction coordinate.

Results

Fourier transform infrared spectroscopy (FTIR)

In addition to their detection in the ISM, both methylamine and methanol have been observed as reaction products in astrochemical ice simulation experiments and are deposited here to form a model ice.[45–47] Ices are prepared in the laboratory by simultaneously depositing pure methanol and pure methylamine from the gas phase onto a silver substrate maintained at 5 K. These ices are characterized *via* FTIR and then irradiated by exposure to 5 keV electrons resulting in an absorbed dose of about 0.6 eV per reactant molecule (Tables S5 and S6); this equates to exposure of ices to a simulated 1–2 million years within a dense molecular cloud with an expected lifetime of 10–50 million years.[51] A low irradiation dose is essential for a comparison to observed astrophysical ices because of the relatively short life-times of molecular clouds and the complexity of these reactants makes them more likely to be found in clouds nearer the end of their life, and only reactions that are achievable within the lifetime of the cloud are of interest here. FTIR spectra are recorded continuously during irradiation and averaged over each two-minute period. The spectra recorded before and after irradiation demonstrate that irradiation results in only small changes between these spectra (Fig. 2), largely seen in the profile of the CH/NH/OH stretching region (2800–3800 cm^{-1}).[64] There are no new absorptions that can be used to identify the presence of reaction intermediates (**A–D**) or products (**1–4**). Due to the complex mixture of trace molecular species produced and their overlapping spectra, FTIR is limited in its ability to provide structure- and formula-specific molecular identification in this model ice. Clear identification of product molecules formed in the ice requires more sensitivity in addition to separation according to both sublimation temperature and mass. Here, this is offered by photoionization reflectron time-of-flight mass spectrometry (PI-ReToF-MS).[65]

Photoionization reflectron time-of-flight mass spectrometry (PI-ReToF-MS)

Photoionization mass spectra collected during temperature programmed desorption (TPD) are shown as a function of temperature in Fig. 3A–D. Experiment were conducted with the CD_3OH–CH_3NH_2 ices recorded at 9.45, 8.89, and 8.45 eV, the CH_3OH–CH_3NH_2 ices recorded at 8.95 and 8.61 eV, and the CD_3OD–CD_3ND_2 ice recorded at 8.89 eV. The sublimation of methylamine at 130–140 K provides a physical mechanism by which other molecules can be delivered into the gas phase. Co-sublimation of reaction products with the methylamine matrix at these temperatures is observed with photoionization at 9.45 and 8.95 eV. Because ionization energy changes with structure, calculations of the adiabatic ionization energies of **1–4** were carried out with the CBS-QB3[43,44] level of theory for each possible conformational isomer (Tables S1–S4). A molecule's adiabatic ionization energy is the lowest photon energy at which ionization is possible, allowing photoionization to be implemented as a structure sensitive probe by varying the photon energy (Fig. 1). Each species is then uniquely identifiable according to its mass, ionization energy, sublimation temperature, and molecular formula as determined by isotopic substitution experiments. The photon energies employed here for single-photon photoionization are too low to produce doubly charged cations, making m/z simply equal to mass (amu), and provide soft ionization (fragmentation-free) such that ions are detected according to the molecular mass of the intact desorbed species.

TPD of irradiated ices mimics the slow warm-up experienced by molecular clouds as they transition into star-formation and allows the molecules contained in the ice to be gradually desorbed into the gas phase. The predicted ionization energy of ethanolamine (**1**) (IE = 8.62–8.93 eV) means that it should be observable with photoionization at 8.95 eV and above but cannot be detected with photons of 8.61 eV. Irradiation and photoionization at 8.95 and 8.89 eV both exhibit a single Gaussian peak in the TPD profile centered at 180 K (Fig. 3C). Since this peak is observable with both 8.95 and 8.89 eV photoionization, it cannot be assigned to **3** (IE = 8.96–9.33 eV). The 180 K peak is not detected at 8.61 eV, and it cannot be assigned

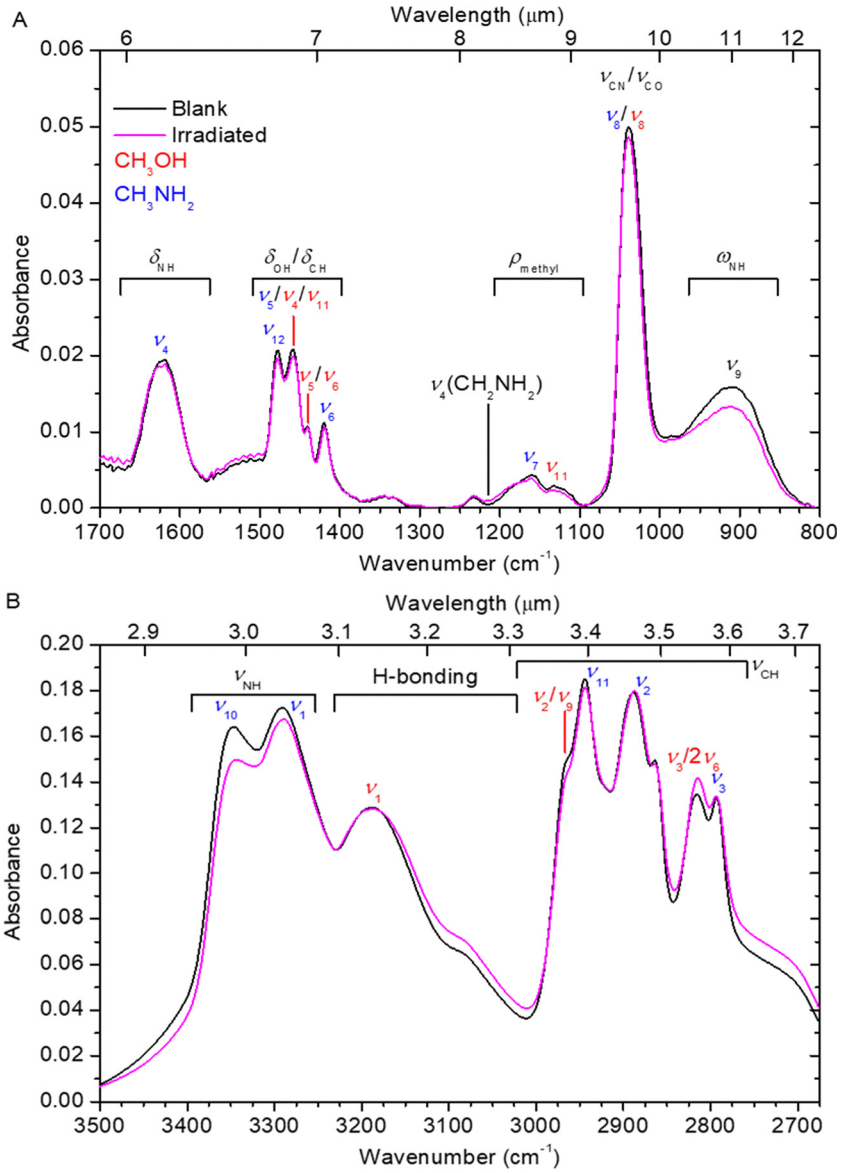

Fig. 2 Fourier transform infrared (FTIR) spectra of methanol–methylamine ice before and after irradiation displaying (A) the 1700–800 cm^{-1} region and (B) 3500–2725 cm^{-1} region.

to **2** (IE = 7.89–8.24 eV) or **4** (IE = 8.33–8.60 eV), leaving ethanolamine (**1**) as the only possible identity of this peak.

The peak at m/z = 61 is presumed to represent C_2H_7NO and can be reproduced with photoionization at 8.89 eV, and again at m/z = 63 with methanol-d_3 (CD_3OH) isotopically substituted ices due to reactions of the hydroxymethyl-d_2 radical ($\dot{C}D_2OH$) derived from methanol-d_3 resulting in isotopically labeled **1**-d_2 ($HOCD_2CH_2NH_2$) (Fig. 3D and Fig. S1 and S2). Detection of this signal at m/z = 63 demonstrates that the carbon of methanol along with two of its hydrogens are incorporated into the product. An additional experiment without irradiation (blank experiment) was conducted at 9.45 eV for CD_3OH–CH_3NH_2 ice; no sublimation event of m/z = 63 was observed in the ethanolamine (**1**) sublimation range (160–220 K) (Fig. 3B), indicating that ethanolamine (**1**) is formed through the electron irradiation of the ices. Full deuteration of both reactants reproduces this peak by production of **1**-d_7 ($DOCD_2CD_2ND_2$) at m/z = 68 (Fig. 3D, Fig. S3). The only possible closed-shell molecular formulae possible containing only atoms of C, H, O, and N and seven hydrogen atoms are H_7N_3—which contains no carbon—and the only plausible formula, C_2H_7NO. Note that in the fully deuterated CD_3OD–CD_3ND_2 ice experiment, the higher irradiation dose (40 nA, 30 min) promotes secondary reaction pathways. The additional sublimation event peaking at around 206 K may be due to the detection of additional C_2H_7NO isomers or other products that shift to the m/z = 68 channel. The repeated observation of the signal attributed to ethanolamine (**1**) at the mass corresponding to the isotopically-substituted molecular formula serves as conclusive evidence that this signal has both the

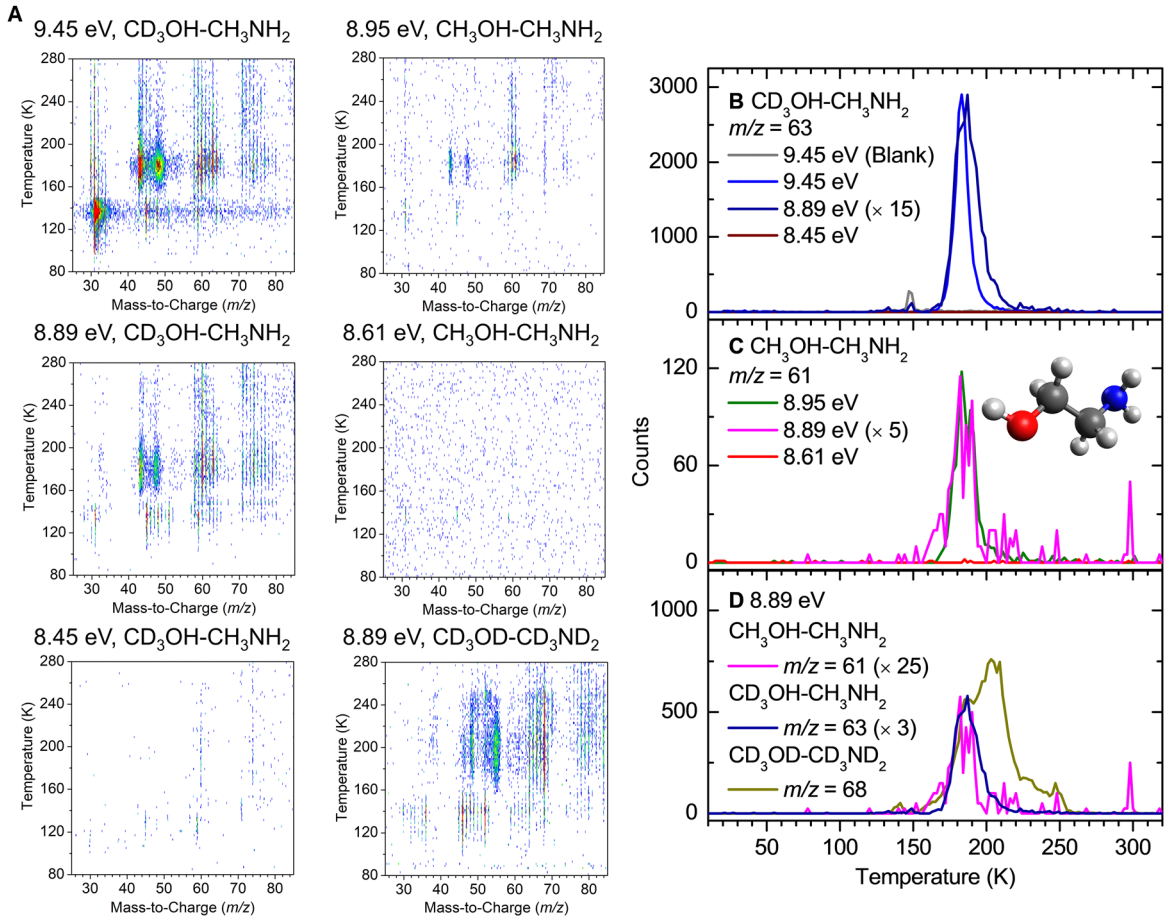

Fig. 3 (A) Photoionization reflectron time-of-flight mass spectrometry (PI-ReToF-MS) two-dimensional traces plotted as a function of both mass and temperature. (B) TPD profiles of m/z = 63 from CD_3OH–CH_3NH_2 ices recorded at 9.45, 8.89, and 8.45 eV. (C) TPD profiles of m/z = 63 from irradiated CH_3OH–CH_3NH_2 ices recorded at 8.95, 8.89, and 8.61 eV. (D) TPD profile of m/z = 68 from irradiated CD_3OD–CD_3ND_2 ice recorded at 8.89 eV, reproducing the peak at 180 K observed with regular and partially deuterated reagents.

ionization energy and molecular formula of ethanolamine (**1**), thus confirming its identity.

Discussion

The isomer-selective production of ethanolamine (**1**) represents the formation of the only biologically active product among accessible C_2H_7NO isomers, and why this should be the case bears scrutiny. Reactions (1a) and (1b) describe the GCR initiated dissociation of methanol leading to hydroxymethyl (**A**, $\dot{C}H_2OH$) and methoxy (**B**, $CH_3\dot{O}$) radicals while reactions (2a) and (2b) describe dissociation of methylamine to the aminomethyl (**C**, $\dot{C}H_2NH_2$) and methylamino (**D**, $CH_3\dot{N}H$) radicals.[66]

$$CH_3OH \rightarrow \dot{C}H_2OH\ (\mathbf{A}) + \dot{H}\ (\Delta_r H^\circ(0\ K) = 184.3 \pm 0.4\ kJ\ mol^{-1}) \quad (1a)$$

$$CH_3OH \rightarrow CH_3\dot{O}\ (\mathbf{B}) + \dot{H}\ (\Delta_r H^\circ(0\ K) = 222.8 \pm 0.5\ kJ\ mol^{-1}) \quad (1b)$$

$$CH_3NH_2 \rightarrow \dot{C}H_2NH_2\ (\mathbf{C}) + \dot{H}\ (\Delta_r H^\circ(0\ K) = 165.9 \pm 0.4\ kJ\ mol^{-1}) \quad (2a)$$

$$CH_3NH_2 \rightarrow CH_3\dot{N}H\ (\mathbf{D}) + \dot{H}\ (\Delta_r H^\circ(0\ K) = 194.4 \pm 0.5\ kJ\ mol^{-1}) \quad (2b)$$

These reactions are all endoergic by about 2 eV but should all be readily initiated by 5 keV electrons (4.8×10^5 kJ mol^{-1}) carrying kinetic energy in excess of any covalent bond. Reactions (1a) and (2a) are both thermodynamically preferred over (1b) and (2b) and both yield carbon-centered radicals; however, the 30–40 kJ mol^{-1} increase in energy needed to produce an oxygen- or nitrogen-centered radical is negligible in comparison to the energy of the incident electrons. The relative stability of the carbon-centered radical alone cannot justify their exclusive production. We inductively presume that these reactions are all possible and investigate the fate of the reactive intermediates produced.

The PI-ReToF-MS technique has demonstrated the ability to identify a variety of unstable organics in the gas phase which are formed only in trace quantities within model ices. Methanediol ($CH_2(OH)_2$)[67] and methanolamine (NH_2CH_2OH),[68] for example, are formed by reactions of radical intermediate **A**. Pure methanol ices have been found to form ethylene glycol (**A_2**, $HOCH_2CH_2OH$), methoxymethanol (**AB**, $HOCH_2OCH_3$),

and dimethylperoxide ($\mathbf{B_2}$, CH_3OOCH_3) which serve as evidence that both **A** and **B** can both be produced in irradiated ices. Methanediamine ($CH_2(NH_2)_2$)[69] has been formed by reactions of **C** and pure methylamine ices yield 1,2-diaminoethane ($\mathbf{C_2}$, $NH_2CH_2CH_2NH_2$); however, there is not yet evidence for production of 1,2-dimethylhydrazine ($\mathbf{D_2}$, $CH_3NH_2NH_2CH_3$) in pure methylamine ices. The production of ethanolamine (**1**) *via* reaction (3) demonstrates that **A** and **C** are present as reaction intermediates, while the absence of a detectable quantity of isomers **2–4** indicates that reactions (4)–(6) do not occur. This must then be due to the absence of one or more reactants because radical–radical recombination reactions are barrierless between simple radicals where the spin density is localized at a particular atom, which is the case for all radicals considered here. It is worth noting that the radical–radical recombination can form ethanolamine (**1**) either during irradiation at 5 K or during TPD at higher temperatures; however, our results cannot distinguish between these two formation mechanisms. As methanol and methylamine desorb prior to the sublimation of ethanolamine (**1**) (Fig. S4), gas-phase formation of ethanolamine (**1**) after sublimation can be ruled out.

$$\dot{C}H_2OH\ (\mathbf{A}) + \dot{C}H_2NH_2\ (\mathbf{C}) \rightarrow H_2NCH_2CH_2OH\ (\mathbf{1})\ (\Delta_r H^\circ(0\ \mathrm{K}) = -190 \pm 11\ \mathrm{kJ\ mol^{-1}}) \quad (3)$$

$$CH_3\dot{O}\ (\mathbf{B}) + CH_3\dot{N}H\ (\mathbf{D}) \rightarrow CH_3NHOCH_3\ (\mathbf{2})\ (\Delta_r H^\circ(0\ \mathrm{K}) = -85 \pm 13\ \mathrm{kJ\ mol^{-1}}) \quad (4)$$

$$\dot{C}H_2NH_2\ (\mathbf{C}) + CH_3\dot{O}\ (\mathbf{B}) \rightarrow CH_3OCH_2NH_2\ (\mathbf{3})\ (\Delta_r H^\circ(0\ \mathrm{K}) = -204 \pm 13\ \mathrm{kJ\ mol^{-1}}) \quad (5)$$

$$CH_3\dot{N}H\ (\mathbf{D}) + \dot{C}H_2OH\ (\mathbf{A}) \rightarrow CH_3NHCH_2OH\ (\mathbf{4})\ (\Delta_r H^\circ(0\ \mathrm{K}) = -204 \pm 12\ \mathrm{kJ\ mol^{-1}}) \quad (6)$$

To provide a qualitative explanation of the experimental results, the reaction potential energy profiles were investigated computationally with explicit representation of up to three total solvating molecules of methanol and/or methylamine and including implicit solvent modelling within a polarized continuum (PCM), which is well-suited to identifying the effects of solvation on reaction thermochemistry and mechanism. Reactions (7)–(9) describe some available destructive pathways for radicals **B** and **D** while the effects of solvation upon these reactions are described by Fig. 4.

$$\dot{C}H_2OH\ (\mathbf{A}) \leftrightarrow CH_3\dot{O}\ (\mathbf{B}) \quad (7)$$

$$\dot{C}H_2NH_2\ (\mathbf{C}) \leftrightarrow CH_3\dot{N}H\ (\mathbf{D}) \quad (8)$$

$$CH_3\dot{O}\ (\mathbf{B}) + CH_3NH_2 \leftrightarrow CH_3OH + CH_3\dot{N}H\ (\mathbf{D}) \quad (9)$$

The potential energy surface represented by these reactions was explored with ωB97X-D/6-311G(d,p) level of theory (Tables S7 and S8) and the identified minimum energy pathways are discussed here after varying both the identity of the solvent molecules (methanol/methylamine) and conformation. Gas-phase isomerization between **A** and **B** in reaction (7) faces a substantial barrier (Fig. 4A), and both radicals are stable in isolation. The addition of a solvating molecule of methanol or methylamine reduces the barrier height (E_{TS}) by up to 46 kJ mol^{-1} and increases the energy of **B** relative to **A** (ΔE) by a further 25 kJ mol^{-1}. Addition of more explicitly represented solvent molecules increases the magnitude of these effects so with three solvating molecules the barrier for the hydrogen shift that converts between **B** to **A** is indistinguishable from zero at this level of theory, 6 ± 10 kJ mol^{-1}. Isomerization between **C** and **D** in reaction (8) responds to solvation similarly (Fig. 4B) where E_{TS} decreases monotonically with increasing solvation and ΔE increases. Reaction (9) displays the opposite response to solvation, where additional molecules of methanol or methylamine increase the stability of the **D** (decreasing ΔE) while increasing E_{TS}.

The polarizable continuum model (PCM) is a widespread method of simulating the implicit effects of electrostatic interaction with the dipole and polarization of nearby molecules.[60] Solvents were modeled using the electrostatic parameters of liquid methanol,[61] solid methanol,[62] and liquid methylamine[63] (Tables S7 and S8). This method of approximating the implicit solvation effects does not reproduce the effects of solvation on E_{TS} & ΔE in calculations where only the reacting molecule is treated at the ωB97X-D/6-311G(d,p) level of theory (Fig. 4) without including explicit solvent molecules. These calculations show that explicit quantum chemical representation of solvating molecules is necessary. Inclusion of both implicit and explicit solvation in calculations results in further reduction of E_{TS} without significant changes in ΔE.

Investigations by Radom and coworkers have identified a related phenomenon and show that proximity to electron withdrawing groups within a molecule can increase the barrier to intermolecular hydrogen abstraction while lowering the energy of some radical sites.[73] Similar behavior is observed here in the intermolecular hydrogen abstraction between methoxy radical and methylamine shown in Fig. 4C, reaction (9). The resulting accumulation of carbon-centered radicals **A** and **C** rather than their oxygen- or nitrogen-centered counterparts **B** and **D** is an efficient route to the selective production of ethanolamine (**1**). In the meantime, besides thermodynamic control, radical distributions may be strongly influenced by the kinetic and dynamic factors, such as dissociation cross sections, energy partitioning, and competing ionization or excitation processes, even under high energy irradiation conditions.

Conclusion

Here, we present the first synthesis of ethanolamine in model interstellar ices and its identification in the gas phase after it sublimes during temperature-programmed desorption. Selective production of only ethanolamine (**1**) among the C_2H_7NO isomers suggests that that its formation mechanism involves recombination of hydroxymethyl ($\dot{C}H_2OH$) and aminomethyl ($\dot{C}H_2NH_2$) radicals in ice mixtures. These intermediates can be produced by the reactants used here which are widespread on the astronomical scale; methanol is quite abundant in interstellar ices, comprising up to 30% relative to water[74–77] and

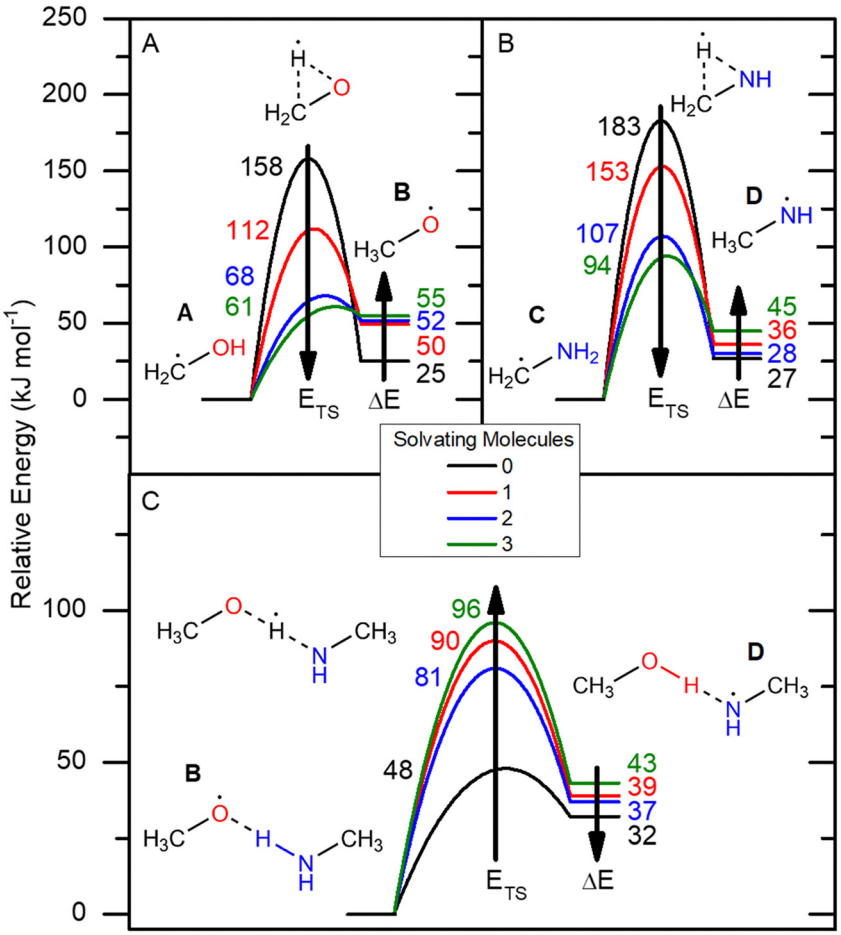

Fig. 4 Minimum energetic barriers (E_{TS}) and relative energy (ΔE) for intramolecular hydrogen transfer in (A) reaction (7) for methanol-derived radicals, (B) reaction (8) for methylamine-derived radicals, and (C) reaction (9) intermolecular hydrogen abstraction were studied at the ωB97X-D/6-311G(d,p)[70,71] level of theory (barrier height error ± 10 kJ mol^{-1})[72] in the gas-phase and with increasing solvation. The contributions from implicit PCM solvent modeling and the effects of varying the identity of the solvating molecules are available in Tables S7 and S8.

methylamine is observed with typical upper limits of 5% relative to water.[78] Furthermore, these intermediates can be formed by respective Ḣ addition to formaldehyde (H_2CO) or methanimine (H_2CNH). Because ethanolamine (**1**) has a large dipole moment—making it readily detected by radioastronomy—and its presence in all forms of life, it is a promising candidate as a marker for prebiotic chemistry in the interstellar medium, *i.e.*, the presence of ethanolamine (**1**) in space may indicate astrochemistry with the potential to lead to life. Furthermore, infrared astronomy has the demonstrated ability to detect methanol and methylamine in interstellar ices, and the local concentration of these reagents serves as an indicator that a molecular cloud contains or has the material required to produce ethanolamine. In interstellar ices, methanol and methylamine are typically embedded in water-rich ices, where radical formation and subsequent recombination can be influenced by the surrounding molecules. Competitive reactions with water or other abundant ice constituents may affect the efficiency of ethanolamine (**1**) formation. Future experiments can explore these effects by incorporating water into the ice mixtures. Additionally, although energetic electrons mimic the secondary electrons generated by GCR interactions, interstellar ices are also processed by ultraviolet (UV) photons and X-rays, which can similarly generate radicals and may contribute to ethanolamine (**1**) formation through complementary pathways.

The unanticipated isomer-selectivity of this reaction is a critical finding in the context of the centrality of ethanolamine (**1**) to biochemistry and can be plausibly attributed to the effects of polar solvation. Computational investigation shows that intermolecular hydrogen abstraction between electron-withdrawing groups is inhibited in the presence of polar molecules while intramolecular hydrogen transfer is facilitated in this environment. A deeper understanding of the extent to which this effect results in isomer-selectivity of radical-radical recombination reactions should prove to be transformative knowledge in the investigation of the interstellar origins of life. Preferential formation of ethanolamine (**1**) may be representative of a tendency toward production of new carbon–carbon bonds in polar ices. Future investigations shall aim to better target the effects of the ice composition on radical intermediate stability. Identifying the necessary conditions that preselect for the formation of ethanolamine (**1**) can guide astronomical

searches for the conditions needed for the origins of life. The heat released during star formation causes small organics to sublime while more complex molecules remain trapped in ices that are incorporated into bodies that comprise a protoplanetary disc. During the earliest period in which the Earth was geologically stable, the Archean Eon beginning some 4 billion years ago, delivery of ethanolamine (**1**) and other necessary organics derived from ices in the interstellar medium was likely a crucial contributor to the chemical primitive lifeforms relied on.

Conflicts of interest

The authors declare no conflict of interest.

Data availability

Essential data are provided in the main text and the supplementary information (SI). Supplementary information: experimental and computational details & methods, reaction schemes for isotopically labelled ices, and computed results including: energetics, structures, and vibrational frequencies. See DOI: https://doi.org/10.1039/d5cp04639d.

Additional data are available from the corresponding author upon reasonable request.

Acknowledgements

The experiments at the University of Hawaii were supported by the United States National Science Foundation (NSF) Division of Astronomical Sciences (NSF AST 2403867). The W. M. Keck Foundation and the University of Hawaii at Manoa financed the construction of the experimental setup.

References

1 N. Balucani, C. Ceccarelli and V. Taquet, *Mon. Not. R. Astron. Soc. Lett.*, 2015, **449**, L16–L20.
2 J. E. Vance, *J. Lipid Res.*, 2008, **49**, 1377–1387.
3 N. Kitadai and S. Maruyama, *Geosci. Front.*, 2018, **9**, 1117–1153.
4 P. A. Weinhold and V. B. Rethy, *Biochem.*, 1974, **13**, 5135–5141.
5 C. R. McMaster and R. M. Bell, *Biochim. Biophys. Acta*, 1997, **1348**, 117–123.
6 J. E. Vance and G. Tasseva, *Biochim. Biophys. Acta, Mol. Cell Biol. Lipids*, 2013, **1831**, 543–554.
7 X. H. Jin, Y. Okamoto, J. Morishita, K. Tsuboi, T. Tonai and N. Ueda, *J. Biol. Chem.*, 2007, **282**, 3614–3623.
8 W. A. Devane, L. Hanus, A. Breuer, R. G. Pertwee, L. A. Stevenson, G. Griffin, D. Gibson, A. Mandelbaum, A. Etinger and R. Mechoulam, *Science*, 1992, **258**, 1946–1949.
9 M. Bogdanov, J. Sun, H. R. Kaback and W. Dowhan, *J. Biol. Chem.*, 1996, **271**, 11615–11618.
10 W. Dowhan and M. Bogdanov, *Biochim. Biophys. Acta*, 2012, **1818**, 1097–1107.
11 B. A. Bladergroen and L. M. van Golde, *Biochim. Biophys. Acta*, 1997, **1348**, 91–99.
12 A. K. Menon and V. L. Stevens, *J. Biol. Chem.*, 1992, **267**, 15277–15280.
13 B. San Francisco, X. Zhang, K. Whalen and J. Gerlt, *FASEB J.*, 2015, **29**, 573-45.
14 E. Miedema and K. E. Richardson, *Plant Physiol.*, 1966, **41**, 1026–1030.
15 J. Zhou, X. Xiong, K. Wang, L. Zou, D. Lv and Y. Yin, *Curr. Mol. Med.*, 2017, **17**, 92–99.
16 K. D. Chapman, *Chem. Phys. Lipids*, 2000, **108**, 221–229.
17 D. Coulon, L. Faure, M. Salmon, V. Wattelet and J. J. Bessoule, *Biochimie*, 2012, **94**, 75–85.
18 M. Serra and J. D. Saba, *Adv. Enzyme Regul.*, 2010, **50**, 349–362.
19 B. W. Carroll and D. A. Ostlie, *An Introduction to Modern Astrophysics*, Cambridge University Press, Cambridge, United Kingdom, 2017.
20 C. Puzzarini and S. Alessandrini, *ACS Cent. Sci.*, 2024, **10**, 13–15.
21 P. D. Holtom, C. J. Bennett, Y. Osamura, N. J. Mason and R. I. Kaiser, *Astrophys. J.*, 2005, **626**, 940–952.
22 C. Zhang, V. Leyva, J. Wang, A. M. Turner, M. McAnally, A. Herath, C. Meinert, L. A. Young and R. I. Kaiser, *Proc. Natl. Acad. Sci. U. S. A.*, 2024, **121**, e2320215121.
23 J. E. Elsila, J. P. Dworkin, M. P. Bernstein, M. P. Martin and S. A. Sandford, *Astrophys. J.*, 2007, **660**, 911–918.
24 S. L. Widicus, B. J. Drouin, K. A. Dyl and G. A. Blake, *J. Mol. Spec.*, 2003, **217**, 278–281.
25 V. K. Kaushik and R. C. Woods, *Z. Phys. Chem.*, 1982, **132**, 117–120.
26 R. E. Penn and R. F. Curl, *J. Chem. Phys.*, 1971, **55**, 651–658.
27 M. K. Sharma, M. Sharma and S. Chandra, *Astron. Nachr.*, 2018, **339**, 306–311.
28 E. S. Wirström, P. Bergman, Å. Hjalmarson and A. Nummelin, *Astron. Astrophys.*, 2007, **473**, 177–180.
29 R. Briggs, G. Ertem, J. P. Ferris, J. M. Greenberg, P. J. McCain, C. X. Mendoza-Gomez and W. Schutte, *Orig. Life Evol. Biosph.*, 1992, **22**, 287–307.
30 V. M. Rivilla, I. Jimenez-Serra, J. Martin-Pintado, C. Briones, L. F. Rodriguez-Almeida, F. Rico-Villas, B. Tercero, S. Zeng, L. Colzi, P. de Vicente, S. Martin and M. A. Requena-Torres, *Proc. Natl. Acad. Sci. U. S. A.*, 2021, **118**, e2101314118.
31 W. A. Schutte, *Adv. Space Res.*, 1995, **16**, 53–60.
32 C. Meinert, I. Myrgorodska, P. de Marcellus, T. Buhse, L. Nahon, V. Hoffmann Søren, S. d'Hendecourt Louis Le and J. Meierhenrich Uwe, *Science*, 2016, **352**, 208–212.
33 P. de Marcellus, C. Meinert, I. Myrgorodska, L. Nahon, T. Buhse, S. d'Hendecourt Lle and U. J. Meierhenrich, *Proc. Natl. Acad. Sci. U. S. A.*, 2015, **112**, 965–970.
34 J. Wang, J. H. Marks, R. C. Fortenberry and R. I. Kaiser, *Sci. Adv.*, 2024, **10**, eadl3236.
35 R. I. Kaiser, S. Maity and B. M. Jones, *Angew. Chem. Int. Ed.*, 2015, **54**, 195–200.
36 M. Nuevo, J. H. Bredehöft, U. J. Meierhenrich, L. d'Hendecourt and W. H.-P. Thiemann, *Astrobiology*, 2010, **10**, 245–256.

37 A. M. Turner, A. Bergantini, M. J. Abplanalp, C. Zhu, S. Gobi, B. J. Sun, K. H. Chao, A. H. H. Chang, C. Meinert and R. I. Kaiser, *Nat. Commun.*, 2018, **9**, 3851.

38 C. Zhu, A. M. Turner, M. J. Abplanalp, R. I. Kaiser, B. Webb, G. Siuzdak and R. C. Fortenberry, *Astrophys. J.*, 2020, **899**, L3.

39 J. M. Hollis, F. J. Lovas and P. R. Jewell, *Astrophys. J.*, 2000, **540**, L107–L110.

40 D. P. Glavin, A. D. Aubrey, M. P. Callahan, J. P. Dworkin, J. E. Elsila, E. T. Parker, J. L. Bada, P. Jenniskens and M. H. Shaddad, *Meteorit. Planet. Sci.*, 2010, **45**, 1695–1709.

41 B. M. Jones and R. I. Kaiser, *J. Phys. Chem. Lett.*, 2013, **4**, 1965–1971.

42 Y. Mo, J. Yang and G. Chen, *J. Chem. Phys.*, 2004, **120**, 1263–1270.

43 J. A. Montgomery, M. J. Frisch, J. W. Ochterski and G. A. Petersson, *J. Chem. Phys.*, 1999, **110**, 2822–2827.

44 J. A. Montgomery, M. J. Frisch, J. W. Ochterski and G. A. Petersson, *J. Chem. Phys.*, 2000, **112**, 6532–6542.

45 N. Fourikis, K. Takagi and M. Morimoto, *Astrophys. J.*, 1974, **191**, L139.

46 N. Kaifu, M. Morimoto, K. Nagane, K. Akabane, T. Iguchi and K. Takagi, *Astrophys. J.*, 1974, **191**, L135.

47 J. A. Ball, C. A. Gottlieb, A. E. Lilley and H. E. Radford, *Astrophys. J.*, 1970, **162**, L203.

48 R. I. Kaiser, *Chem. Rev.*, 2002, **102**, 1309–1358.

49 A. M. Turner, M. J. Abplanalp, S. Y. Chen, Y. T. Chen, A. H. H. Chang and R. I. Kaiser, *Phys. Chem. Chem. Phys.*, 2015, **17**, 27281–27291.

50 R. L. Hudson, Y. Y. Yarnall and P. A. Gerakines, *Astrobiology*, 2022, **22**, 452–461.

51 A. G. Yeghikyan, *Astrophysics*, 2011, **54**, 87–99.

52 D. Drouin, A. R. Couture, D. Joly, X. Tastet, V. Aimez and R. Gauvin, *Scanning*, 2007, **29**, 92–101.

53 M. J. Frisch, G. W. Trucks, H. B. Schlegel, G. E. Scuseria, M. A. Robb, J. R. Cheeseman, G. Scalmani, V. Barone, B. Mennucci, G. A. Petersson, H. Nakatsuji, M. Caricato, X. Li, H. P. Hratchian, A. F. Izmaylov, J. Bloino, G. Zheng, J. L. Sonnenberg, M. Hada, M. Ehara, K. Toyota, R. Fukuda, J. Hasegawa, M. Ishida, T. Nakajima, Y. Honda, O. Kitao, H. Nakai, T. Vreven, J. A. M. Jr., J. E. Peralta, F. Ogliaro, M. Bearpark, J. J. Heyd, E. Brothers, K. N. Kudin, V. N. Staroverov, T. Keith, R. Kobayashi, J. Normand, K. Raghavachari, A. Rendell, J. C. Burant, S. S. Iyengar, J. Tomasi, M. Cossi, N. Rega, J. M. Millam, M. Klene, J. E. Knox, J. B. Cross, V. Bakken, C. Adamo, J. Jaramillo, R. Gomperts, R. E. Stratmann, O. Yazyev, A. J. Austin, R. Cammi, C. Pomelli, J. W. Ochterski, R. L. Martin, K. Morokuma, V. G. Zakrzewski, G. A. Voth, P. Salvador, J. J. Dannenberg, S. Dapprich, A. D. Daniels, O. Farkas, J. B. Foresman, J. V. Ortiz, J. Cioslowski and D. J. Fox, *Gaussian 09, Revision D.1*, Gaussian, Inc., Wallingford CT, 2009.

54 T. B. Adler, G. Knizia and H.-J. Werner, *J. Chem. Phys.*, 2007, **127**, 221106.

55 G. Knizia, T. B. Adler and H.-J. Werner, *J. Chem. Phys.*, 2009, **130**, 054104.

56 S. Grimme, *J. Chem. Phys.*, 2006, **124**, 034108.

57 S. Grimme, S. Ehrlich and L. Goerigk, *J. Comput. Chem.*, 2011, **32**, 1456–1465.

58 L. Goerigk and S. Grimme, *J. Chem. Theory Comput.*, 2011, **7**, 291–309.

59 H. Werner, P. Knowles, G. Knizia, F. Manby, M. Schütz, P. Celani, W. Györffy, D. Kats, T. Korona and R. Lindh, *MOLPRO 2015*, University of Cardiff Chemistry Consultants (UC3) Cardiff, Wales, UK, 2015, https://www.molpro.net.

60 G. Scalmani and M. J. Frisch, *J. Chem. Phys.*, 2010, **132**, 114110.

61 H. G. Carlson and E. F. Westrum, *J. Chem. Phys.*, 1971, **54**, 1464–1471.

62 D. W. Davidson, *Can. J. Chem.*, 1957, **35**, 458–473.

63 W. T. Cronenwett and L. W. Hoogendoorn, *J. Chem. Eng. Data*, 2002, **17**, 298–300.

64 G. Socrates, *Infrared and Raman Characteristic Group Frequencies: Tables and Charts*, Wiley, Chichester, 2004.

65 M. J. Abplanalp, M. Förstel and R. I. Kaiser, *Chem. Phys. Lett.*, 2016, **644**, 79–98.

66 B. Ruscic and D. Bross, *Active Thermochemical Tables (ATcT) values based on ver. 1.130 of the Thermochemical Network*. Argonne National Laboratory, Lemont, Illinois, 2023, available at https://ATcT.anl.gov. 2023.

67 C. Zhu, N. F. Kleimeier, M. Turner Andrew, K. Singh Santosh, C. Fortenberry Ryan and I. Kaiser Ralf, *Proc. Natl. Acad. Sci. U. S. A.*, 2022, **119**, e2111938119.

68 S. K. Singh, C. Zhu, J. La Jeunesse, R. C. Fortenberry and R. I. Kaiser, *Nat. Commun.*, 2022, **13**, 375.

69 J. H. Marks, J. Wang, R. C. Fortenberry and R. I. Kaiser, *Proc. Natl. Acad. Sci. U. S. A.*, 2022, **119**, e2217329119.

70 J. D. Chai and M. Head-Gordon, *Phys. Chem. Chem. Phys.*, 2008, **10**, 6615–6620.

71 R. Krishnan, J. S. Binkley, R. Seeger and J. A. Pople, *J. Chem. Phys.*, 1980, **72**, 650–654.

72 N. Mardirossian and M. Head-Gordon, *Mol. Phys.*, 2017, **115**, 2315–2372.

73 R. J. O'Reilly, B. Chan, M. S. Taylor, S. Ivanic, G. B. Bacskay, C. J. Easton and L. Radom, *J. Am. Chem. Soc.*, 2011, **133**, 16553–16559.

74 G. J. White, M. Araki, J. S. Greaves, M. Ohishi and N. S. Higginbottom, *Astron. Astrophys.*, 2003, **407**, 589–607.

75 A. Fuente, J. Cernicharo, P. Caselli, C. McCoey, D. Johnstone, M. Fich, T. van Kempen, A. Palau, U. A. Yıldız, B. Tercero and A. López, *Astron. Astrophys.*, 2014, **568**, A65.

76 S. Cazaux, A. G. G. M. Tielens, C. Ceccarelli, A. Castets, V. Wakelam, E. Caux, B. Parise and D. Teyssier, *Astrophys. J.*, 2003, **593**, L51–L55.

77 B. Parise, C. Ceccarelli, A. G. G. M. Tielens, E. Herbst, B. Lefloch, E. Caux, A. Castets, I. Mukhopadhyay, L. Pagani and L. Loinard, *Astron. Astrophys.*, 2002, **393**, L49–L53.

78 M. G. Rachid, N. Brunken, D. de Boe, G. Fedoseev, A. C. A. Boogert and H. Linnartz, *Astron. Astrophys.*, 2021, **653**, A116.

